Contents

1 Wave Localization Transitions in Complex Systems *1*

Jan W. Kantelhardt

Lukas Jahnke

Richard Berkovits

1.1 Introduction *1*

1.2 Complex Networks *3*

1.2.1 Scale-Free and Small-World Networks *3*

1.2.2 Clustering *5*

1.2.3 Percolation on Networks *7*

1.2.4 Simulation of Complex Networks *8*

1.3 Models with Localization-Delocalization Transitions *10*

1.3.1 Standard Anderson Model and Quantum Percolation *10*

1.3.2 Vibrational Excitations and Oscillations *11*

1.3.3 Optical Modes in a Network *13*

1.3.4 Anderson Model with Magnetic Field *14*

1.4 Level Statistics *16*

1.4.1 Random Matrix Theory *16*

1.4.2 Level Statistics for Disordered Systems *17*

1.4.3 Corrected Finite-Size Scaling *19*

1.4.4 Finite-Size Scaling with Two Parameters *20*

1.5 Localization-Delocalization Transitions in Complex Networks *21*

1.5.1 Percolation Networks *21*

1.5.2 Small-World Networks without Clustering *22*

1.5.3 Scale-Free Networks with Clustering *23*

1.5.4 Systems with Constant and Random Magnetic Field *25*

1.6 Conclusion *26*

Acknowledgement *28*

1
Wave Localization Transitions in Complex Systems

Jan W. Kantelhardt[1)]
Lukas Jahnke
Richard Berkovits[2)]

1.1
Introduction

Phase transitions between localized and extended modes remain in the focus of research on disordered systems although half a century has passed since the localization phenomenon was first reported in the context of electron transport through disordered metals [1, 2]. Such transitions have also been suggested and verified in many physically very different systems, such as light in strongly scattering media [3, 4] or photonic crystals [5, 6], acoustical vibrations in glasses [7] or percolation systems [8], and very recently atomic Bose-Einstein condensates in an aperiodic optical lattice [9, 10].

The main idea is that a phase transition from extended to localized eigenstates exists as a function of the disorder in the system. This Anderson transition will be manifested by a change in the transport through the system, e. g. from metallic to insulating or from transparent to reflecting. The transition is conceptually different from the canonical explanation for the existence of insulators (i. e., the Fermi energy is in the gap between two energy bands), since for an Anderson insulator there are many available states at the Fermi level. Nevertheless, since these eigenstates are localized due to the disorder, no current can pass through the system for electronic systems. In the case of vibrational excitations, propagating phonon modes are replaced by localized excitations, which reduces heat conduction through the material. Localization of light is correspondingly defined, but most difficult to observe experimentally. The reason is that it is hard to distinguish systems with localized light modes from those with strong light absorption, since both effects lead to an exponential decay [3, 4]. This is a motivation for the study of light localization in artificially designed optical systems.

[1)]Institut für Physik, Martin-Luther-Universität Halle-Wittenberg, 06099 Halle (Saale), Germany
[2)]Minerva Center and Department of Physics, Bar-Ilan University, Ramat-Gan 52900, Israel

Another relevant phase transition occurring in disordered systems is the percolation transition. Although both, localization-delocalization transitions (Anderson transitions) and percolation transitions are caused by the disorder of the considered system, they have different origins and can be clearly distinguished. The percolation transition is a purely geometrical transition. When more and more sites become unoccupied or bonds are broken (i. e. the occupation probability is reduced) the large percolation cluster breaks into pieces and direct paths between two edges of the sample disappear. Transport is thus interrupted below the critical percolation threshold, since there are no more paths available. In the Anderson transition, on the other hand, such paths do exist. Nevertheless the probability of waves transversing the sample is exponentially small due to constructive interference between time reversed paths and destructive interference between paths with identical beginning and end. Thus, the Anderson transition takes into account the wave (or quantum) nature of the modes travelling through the sample, while the percolation transition is purely classical in nature.

Since the Anderson transition depends on interference effects between time reversed paths, there is an interesting dependence on the dimensionality of the system. The lower critical dimension, at and below which the system is localized for all strengths of disorder, is believed to be two [11]. The reason is that the probability of returning to the origin stays non-zero in the limit of infinite system size for $d \leq 2$. The upper critical dimension with extended modes remaining for any strength of disorder is still uncertain, although it is generally believed to be infinity [12, 13, 14, 15, 16].

In order to elucidate the causes for the dimensionality dependence of the Anderson transition, studies considering more complex topologies have recently been undertaken. The reason is that several properties of the system (like the probability of short or long paths returning to the origin) can be modified systematically in addition to normal on-site or bond disorder in such systems. Recently, Anderson transitions in small-world networks [17, 18, 19], Cayley trees [20], random regular graphs, Erdös-Rényi graphs and scale-free networks [21, 22] have been studied. In addition to justifying this interest by the light shed on the general properties of the transition, we would like to emphasis that complex networks could be actually realized in real-world situations such as optical networks (see below).

The chapter is organized as follows. We begin with a description of complex networks in Section 1.2, focussing particularly on scale-free networks with and without clustering and with and without additional percolation. Our considered models for transport on the systems, i. e., electronic wave functions with and without magnetic field, vibrational modes, and coherent optical modes are given in Section 1.3. Then we describe how one can determine the properties of an Anderson transition based on the statistical properties of the eigenvalues (levels) of the Hamiltonians or dynamical matrices using level statistics and finite-size scaling in Section 1.4. Results for the Anderson transition in different complex networks are finally reported in Section 1.5 with particular emphasis on effects of clustering. We show that new complex topologies lead to novel physics, specifically increasing clustering may lead to localization even without additional disorder. We summarize and conclude in Section 1.6.

1.2 Complex Networks

Complex networks can be found in a variety of dynamical systems, such as protein folding, food webs, social contacts, phone calls, collaborational networks in science and business, the world wide web (WWW), and the Internet. In a network, one typically speaks of nodes which are linked (connected) through edges. For example, in social networks the nodes are humans and the edges are different types of social connections. In the Internet, the nodes are hubs and servers, while the edges are connections between them. The number of edges a node participates in, is its degree k.

The structure of disordered physical materials can also be described in terms of a network. Prominent examples are the SiO_2 network in a glass or structures of amorphous materials. Here, the fluctuating value of k represents the number of bonds (edges) for each of the atoms (nodes). The main distinction between a general complex network and structural networks in materials is the absence of long-range links in materials. In optical systems coherent propagation of light over long distances can be realized with optical fibers (see Section 1.3.3).

1.2.1 Scale-Free and Small-World Networks

In general it is possible to group complex networks using only few characteristic properties, although the networks can be found in very different applications. A very important characteristic is the distribution of degrees, $P(k)$. In a random graph with N nodes each node is connected to exactly k_0 random neighbors [23]; thus $P(k) = 1$ for $k = k_0$ and zero otherwise. In Erdös-Rényi networks, where N nodes are connected randomly with a probability p, the degree distribution is given by a Poisson distribution peaking at $k_0 = \langle k \rangle = p(N-1)$ [23, 24],

$$P(k) = k_0^k e^{-k_0}/k!. \tag{1.1}$$

For another important class of networks, so called scale-free networks, one finds [25]

$$P(k) = ak^{-\lambda} \quad \text{for } m \leq k \leq K \quad \text{with } \lambda > 2. \tag{1.2}$$

where $a = (\lambda - 1)m^{\lambda-1}$. The upper cutoff value $K = mN^{1/(\lambda-1)}$ depends on the system size N [26]. Such networks are called scale-free, because the second moment, $\langle k^2 \rangle$, diverges in the limit of infinite system size ($N \to \infty$). Hence, no intrinsic scale k_0 can be defined. Scale-free networks can be found in natural, sociological and technological networks. For example, the Internet is characterized by $\lambda \approx 2.6$ [27].

Figure 1.1 shows representative simulated scale-free networks with $\lambda = 5$. Note that sometimes not all nodes are linked to the largest cluster (giant component), but finite clusters also appear, even if no edges are cut. However, the degree distribution $P(k)$ is practically identical for the giant component and the whole network as

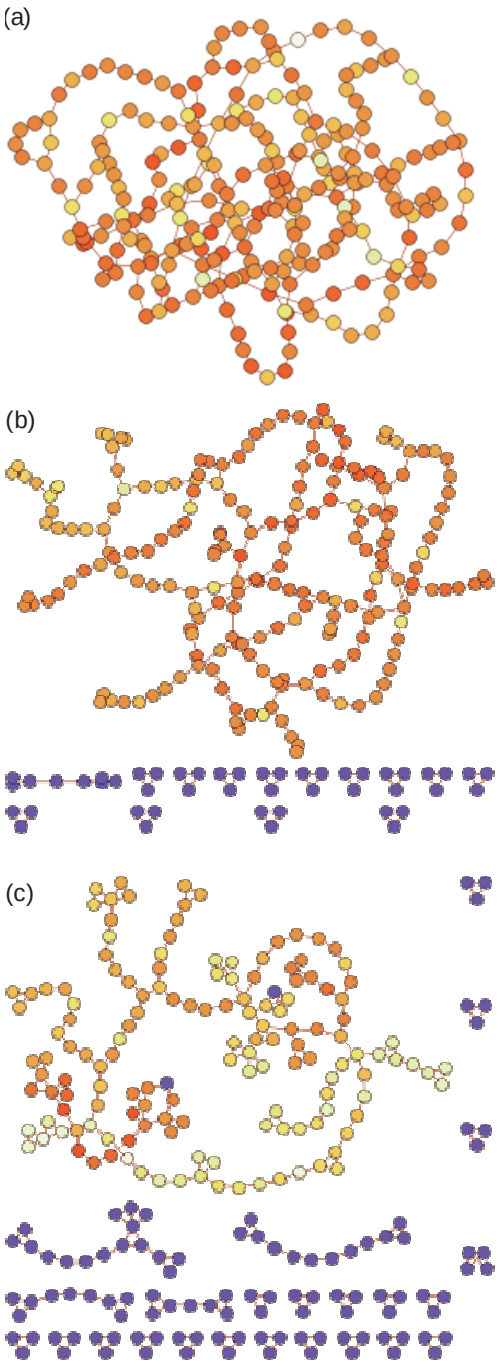

Fig. 1.1 Representative pictures of scale-free networks (degree disgribution exponent $\lambda = 5$) (a) without and (b,c) with clustering ($C_0 = 0.4, 0.6$). All three networks have the same size of $N = 250$. The giant component has a size of (a) $N_g = 250$, (b) $N_g = 203$, and (c) $N_g = 145$. The actual global clustering coefficient is (a) $C = 8 \times 10^{-4}$, (b) $C = 0.34$, and (c) $C = 0.53$. The global clustering coefficient of the giant component is (b) $C_g = 0.10$ and (c) $C_g = 0.17$, since there are several small clusters with larger C. The logarithmically scaled coloring presents the intensity of an optical mode with $E \approx 0.45$, red indicating the highest, yellow intermediate, and blue the lowest intensities.

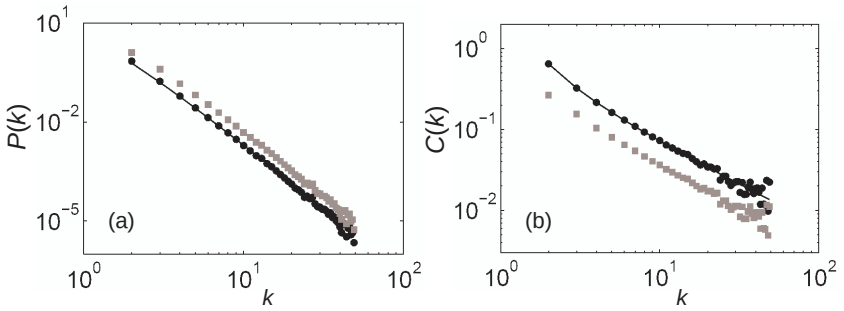

Fig. 1.2 (a) Degree distribution $P(k)$ and (b) degree-dependent clustering coefficients $C(k)$ for scale-free networks with $\lambda = 4$ in (5.2), $C_0 = 0.65$, $\alpha = 1$ according to (5.5), and $N = 15000$ nodes, averaged over 120 configurations. Circles with lines for distributions regarding the whole network and grey squares for the giant component (with $\langle N_1 \rangle = 11906$ nodes; shifted vertically by a factor of 2 for the degree distribution). Figure redrawn after [22].

shown in Fig. 1.2(a) for scale-free networks with $\lambda = 4$. We note that a localization-delocalization transition is well defined only on the giant component since the other clusters do not grow with system size. Just the giant component becomes infinite for an infinite system size. For the finite clusters a localized state with a localization length larger than the cluster size cannot be distinguish from an extended state.

Another important network property is the average path length l. The path length $l_{n,m}$ between nodes n and m is defined as the number of nodes along the shortest path between them. Another way to define the topological size of networks is the diameter d which is the maximal distance between any pair of nodes. For random graphs and Erdös-Rényi graphs the average path length l and the diameter d can be calculated analytically and are given by the logarithm of its size, $l \propto d \propto \ln N$ [23]. The average path length and the diameter of scale-free networks depend on the exponent λ. For $\lambda > 3$ one finds the same results as in the Erdös-Rényi graph case whereas for $\lambda < 3$, $d \propto \ln \ln N$ [28], and for $\lambda = 3$, $d \propto \ln N / \ln \ln N$ [29]. Since the average distance of the nodes is very small, such complex networks are revered to as small-world objects. Moreover, scale-free networks with $\lambda < 3$ are referred to as ultra small-world objects.

Examples of real complex networks are listed in Table 1.1. All presented networks are small-world objects with average path length around three. This average path length is similar for equivalent random networks. However, lattices and other structures without long-range edges do not have short path lengths. For a d-dimensional hypercubic lattice the average path lengths scales as $N^{1/d}$, i. e., it increases much faster with N.

1.2.2 Clustering

Another property observed in real networks is clustering. Especially social networks tend to contain cliques. These are circles of friends or acquaintances where every

Table 1.1 Characteristic quantities of real-world networks: size of considered (sub-) network N, average degree $\langle k \rangle$, average path length l, average path length of an equivalent random network $l_{\rm rand}$, clustering coefficient C, and clustering coefficient of an equivalent random network $C_{\rm rand}$. Data taken from [23].

network	N	$\langle k \rangle$	l	$l_{\rm rand}$	C	$C_{\rm rand}$
WWW, site level	153,127	35.21	3.1	3.35	0.1078	0.00023
Internet, domain level	3015-6209	3.5-4.1	3.7	6.4-6.2	0.18-0.3	0.001
movie actor	225,226	61	3.65	2.99	0.79	0.00027
co-authorship	56,627	173	4.0	2.12	0.726	0.003
co-occurrence of words	460,902	70.13	2.67	3.03	0.437	0.0001

member knows every other member. Such behavior can be quantified by the clustering coefficient C. If the neighbors of a node n with k_n edges are grouped in a clique where everybody is connected with each other, this clique has a total of $k_n(k_n-1)/2$ edges. The clustering coefficient can then be defined as the ratio of the actual number of edges between these nodes, T_n, and the maximum number of possible edges [30],

$$C_n = \frac{2T_n}{k_n(k_n-1)}. \tag{1.3}$$

Here T_n is also the numbers of triangles passing through vertex n. Since each triangle represents a very short loop in the network, waves in networks with high clustering will have a high probability to return to the same node and to interfere destructively. Such interferences are the main reason for quantum localization. One may thus expect that strong clustering in complex networks can induce localization.

Although clustering is by definition a local topological quantity, it is possible to define a global clustering coefficient C by averaging over C_n. Such global approach cannot take into account special properties of a network. For instance different degree-degree correlations, also known as assortativity, can lead to equal C, although the topological structures of the networks are fundamentally different [31, 32, 33, 34]. A practical ansatz is a degree-dependent clustering coefficient [35, 36],

$$\bar{C}(k) = \frac{1}{N_k} \sum_{n \in \Gamma(k)} C_n, \tag{1.4}$$

where N_k is the number of vertices of degree k and $\Gamma(k)$ is the set of such vertices.

It is not possible to achieve all functional dependences of $\bar{C}(k)$ with k. To achieve high clustering of the higher degrees k the assortativity of the network has to be strong. When nodes with large degrees are connected to nodes with lower degrees they cannot achieve a high clustering because the nodes with lower degrees do not have enough connections to participate in a large number of triangles. Depending on the strength of the degree-degree correlation one finds an upper limit which can be approximated by

$$\bar{C}(k) = C_0(k-1)^{-\alpha} \tag{1.5}$$

with α between 1 for no and 0 for high assortativity. Although assortativity is definitely an interesting subject we focus on the effect of clustering here. To prevent interference

between both we keep the degree-degree correlation as low as possible, restricting ourselves to $\alpha = 1$.

The measured clustering coefficients of real networks reported in Table 1.1 are much higher than those of the equivalent random networks, where nearly no cliques emerge. This occurs due to equivalent probabilities for a connection of nearest neighbors and two random nodes [23],

$$C_{\mathrm{rand}} = \langle k \rangle / N, \tag{1.6}$$

decaying to zero for large N. The larger C values in Table 1.1 indicate the presence of many loops on short length scales [23, 37, 38]. Furthermore C is independent of the network size N. This observation bears similarity with a lattice, where clustering is also size independent, depending only on the coordination number.

1.2.3
Percolation on Networks

Percolation is a standard model for disordered systems. Its applications range from transport in amorphous and porous media and composites to the properties of branched polymers, gels and complex ionic conductors. Because of universality the results do not depend on the specific model, and general scaling laws can be deduced. For site percolation on a lattice, each site is occupied randomly with probability p (or it is empty with probability $q = 1 - p$). For a small p all clusters of neighboring occupied sites are finite and transport through the system is impossible. A so-called infinite cluster emerges if p exceeds the critical concentration p_c, where the system undergoes a geometrical phase transition. For $p \geq p_c$ transport through the system is possible and extended modes can occur on the infinite cluster. Besides site percolation, other variants exist, e. g., percolation in continuum space or bond percolation.

Similar to lattices, percolation can be defined on networks. The occupation probability p is equivalent to the probability to connect an edge or to introduce a node. The critical occupation probability p_c of a network depends on its degree distribution. A randomly connected network with arbitrary degree distribution has an infinite cluster if [39, 26, 40]

$$\langle k^2 \rangle / \langle k \rangle > 2. \tag{1.7}$$

Random removal of nodes and edges with probability $q = 1 - p$ changes the degree distribution, reducing $\langle k^2 \rangle / \langle k \rangle$. The critical probability p_c is reached when $\langle k^2 \rangle / \langle k \rangle = 2$. Scale-free networks are particularly interesting, since it is nearly impossible to break them, i. e., $p_c > 0.99$ is found for exponents $2 < \lambda < 3$ [26, 40, 41].

Equation (1.7) is only true for uncorrelated networks with zero clustering. The influence of degree-degree correlations on the stability of networks, however, has not been investigated in much detail. For uncorrelated networks with clustering coefficient C_0, defined in Eq. (1.5), an infinite cluster exists if [32]

$$\langle k^2 \rangle / \langle k \rangle > 2 + C_0. \tag{1.8}$$

Therefore, clustering shifts the percolation threshold, such that the network breaks already for lower values of p. Recently it was found that the network can also be broken by a mere change of the clustering index C without tampering with the degree distribution, i. e., without removing nodes or bonds [22].

1.2.4
Simulation of Complex Networks

The simplest way to create networks with high clustering but small l was proposed by Watts and Strogatz in 1998 [30]. In this model one starts with an ordered ring lattice where each node is connected to the K nodes closest to it. In this ordered case, the clustering coefficient is

$$C = \frac{3(K-2)}{4(K-1)}, \tag{1.9}$$

converging to $3/4$ in the limit of large K. In the second step, the edges are rewired with a probability p_r without allowing self-connections and duplicate edges. Therefore, $p_r NK/2$ long-range edges are introduced, connecting to other neighborhoods. Using this model, it is possible to numerically calculate the dependence of clustering $C(p_r)$ and average path length $l(p_r)$ on the rewiring probability p_r. The transition to a small-world object is rather fast, with nearly a constant clustering coefficient. As a result, the small-world phenomena is almost undetectable at the local level. A coexistence of small-world characteristics and high clustering is thus possible as observed in real world networks (see Table 1.1). However, the Watts-Strogatz model cannot generate scale-free networks, since the degree distribution $P(k)$ decays exponentially.

In the pioneering work of Barabási and Albert [42] it is argued that real networks have two generic mechanisms missing in random graphs. Firstly, real networks grow from a small number of nodes by including new nodes and edges, e. g. the WWW is growing exponentially by new links and additional pages, and co-authorship connections in scientific publications are growing steadily by new publications. Secondly, nodes are not connected independent of their degree, i. e., nodes with high degree are more probable to be linked with new nodes. For example well known web pages, having large number of links, will be linked more often than unknown ones. Just as well, papers with a large number of citations are more likely to be cited again. This phenomena is known as preferential attachment in network science. Both ingredients, growth and preferential attachment, lead to a model which dynamically reproduces scale-free degree distributions [42]. However, the Barabási-Albert model fails to reproduce the strong clustering observed in real complex networks (see Table 1.1).

Therefore we have used an algorithm suggested recently by Serrano and Boguñá [36] which can generate complex small-world networks with predefined degree distribution $P(k)$ *and* predefined degree-dependent clustering coefficients $\bar{C}(k)$. Figure 1.1 shows three representative pictures of the resulting scale-free networks. They all have the same number N of nodes; C_0 increases from (a) to (c). One can clearly see that an increasing number of nodes disintegrate from the giant component for higher clustering. The reason is that for nodes with low degree it is easier to achieve higher clustering

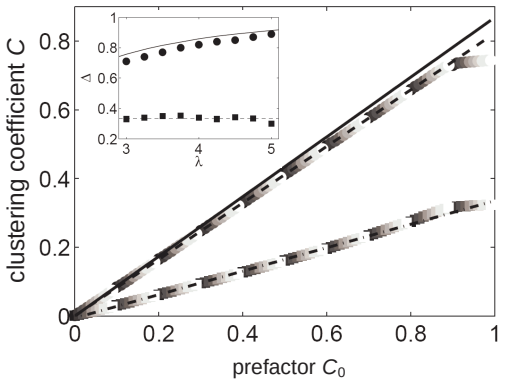

Fig. 1.3 Test of the relation $C = C_0\Delta(\lambda)$ (line) for scale-free networks with $\lambda = 4$ and $m = 2$. The circles (squares) are results for the full network (giant component). The different gray scales represent different system sizes from $N = 2000$ (black) to $N = 20000$ (white). The dashed (dashed dotted) line is a linear fit for the full network (giant component). Inset: Results of the fits for $\Delta(\lambda)$ (same symbols). The full line marks the theoretical maximum Δ for the whole network, while the dashed line marks the average $\langle\Delta\rangle = 0.34$ for the giant component.

in separate small clusters. For example nodes with a degree of two can achieve the highest clustering in triangles.

Figure 1.2(a) confirms that the algorithm can achieve practically identical scale-free degree distributions $P(k)$ for the whole network as well as the giant component. The degree-dependent clustering index $\bar{C}(k)$ for the whole network shown in Fig. 1.2(b) also follows very closely Eq. (1.5) with $\alpha = 1$. However, the values of $\bar{C}(k)$ for the giant component are drastically smaller by approximately a factor between two and three, leading to a reduced global clustering index C_g of the giant component compared with the global clustering index C of the whole network.

It is a-priori not clear if either C or C_g is the better order parameter for studying phase transitions upon increasing clustering. The ambiguity can be resolved by analyzing the dependence of C and C_g on C_0. An illustrative result is shown in Fig. 1.3. Both, C and C_g depend linearly on C_0 if $C_0 \leq 0.9$. We also found no system-size dependence, which is important since we want to use a finite-size scaling formalism to analyze the phase transition. The value of C_0 fed into the network generation algorithm can thus be used as order parameter for studying transitions upon clustering. However, values of $C_0 \geq 0.85$ should avoided since the algorithm fails to achieve such high clustering.

The relation between C and C_0 is characterized by a factor Δ depending mainly on λ, i. e., $C = C_0\Delta(\lambda)$ with $\Delta = \sum_{k=m}^{K}(k-1)P(k)$. The theoretically possible maximum of Δ can be calculated exactly using the basic network parameters (m, K, λ, and N) as well as Eq. (1.2). As shown in the inset of Fig. 1.3 this maximal clustering is very closely reached for a wide range of exponents λ in the degree distribution (compare circles and full line). For the giant component, the prefactor Δ_g linking C_g with C_0 cannot be calculated analytically. It is significantly smaller than the Δ for C, but apparently rather independent of λ as shown in the inset of Fig. 1.3.

We obtained similar, however less reliable results when generating networks using the algorithm of Volz [43] fixing C instead of $\bar{C}(k)$. The problem of this algorithm is that it is not possible to control the assortativity. Therefore the assortativity can change when C is altered, making it difficult to decide whether two networks with different C are comparable.

1.3 Models with Localization-Delocalization Transitions

In this section, models for electrons, vibrational modes and optical modes in disordered systems are described. They are all believed to be in the same universality class and could be supplemented by spin waves. The last part deals with electrons in an additional magnetic field, where the universality class is changed from orthogonal to unitary.

1.3.1 Standard Anderson Model and Quantum Percolation

To study localization effects one can consider the standard Anderson Hamiltonian [1],

$$H = \sum_n \epsilon_n \hat{a}_n^\dagger \hat{a}_n + \sum_{n,\delta}{}' t_{n+\delta,n} \hat{a}_{n+\delta}^\dagger \hat{a}_n, \tag{1.10}$$

with the second sum running over all neighboring pairs of nodes n and $n+\delta$. The operator $\hat{a}_n$ ($\hat{a}_n^\dagger$) is creating (annihilating) a particle at position $\vec{R}_n$. The first part of Eq. (1.10) represents an on-site (node) potential and the second part describes the transfer between the linked pairs of nodes $(n+\delta, n)$. Disorder can be introduced by parametrization of the potential landscape ϵ_n (diagonal disorder) or the hopping-matrix elements $t_{n+\delta,n}$ (off-diagonal disorder). The equation is equivalent with the tight-binding equation for wave function coefficients $\psi_{n,E}$ and energy eigenvalues E,

$$E\psi_{n,E} = \epsilon_n \psi_{n,E} + \sum_\delta{}' t_{n+\delta,n} \psi_{n+\delta,E}. \tag{1.11}$$

Here, we focus on diagonal disorder characterized by an homogeneous uncorrelated distribution of the on-site potentials $-W/2 < \epsilon_n < W/2$. For vanishing disorder strength W and an ordered lattice the energy eigenvalues form energy bands of finite width and the eigenfunctions correspond to periodic Bloch functions spreading the entire system. Electrons in such extended states are highly mobile and contribute to charge transport. For strong disorder (large W) large fluctuations of the potential energy lead to backscattering and interference effects, and the wave function localizes. It decays roughly exponentially in space, although the shape also depends on the averaging procedure (see [44] for details). Therefore electrons are bound at impurities and cannot contribute to transport.

Starting from an ordered lattice, the density of states broadens with increasing disorder and localized states appear near the band edges. They are separated from the extended states in the band center by a critical energy $\pm E_c$ called mobility edge [2]. At a critical disorder W_c the mobility edges merge at $E = 0$ (the band center), and all extended states disappear. At this point a quantum-phase transition occurs, known as the metal-insulator transition. For a one-dimensional system $W_c = 0$ can be derived analytically [2]. For higher dimensions, there are no analytical approaches, and W_c needs to be extracted from numerical simulations. As a result, the properties of two-dimensional systems are discussed somewhat controversially, although no extended

states are usually believed to exist ($W_c = 0$). In three-dimensional systems the phase transition from extended to localized states is observed for $W_c \approx 16.5$ [2, 45, 46].

It needs higher accuracy and a large numerical effort to determine the value of the critical exponent ν characterizing the divergence of the correlation length scale ξ of the wave functions near the phase transition point, $\xi \sim |W - W_c|^{-\nu}$ by a power law. Therefore, the reported values of ν for the standard Anderson model changed as accuracy was improved. The range is from $\nu = 1.2 \pm 0.3$ [2] to $\nu = 1.56 \pm 0.02$ [46].

In the percolation model, disorder is introduced via the (non-diagonal) hopping terms $t_{n+\delta,n}$ that are 1 only if both neighboring sites $n + \delta$ and n are occupied and 0 otherwise. The diagonal terms ϵ_n are usually set to zero. Therefore, the geometrical structure of the considered percolation cluster determines the localization properties of the wave functions. For $p < p_c$ all clusters are finite, and the eigenfunctions are always localized. The same is true at p_c due to the fractal structure of the infinite cluster, resembling a highly disordered system. For $p > p_c$ the infinite cluster becomes more and more dense, until an ordered lattice is reached for $p = 1$ with extended plain waves as eigenfunctions of the tight-binding Hamiltonian. In between a critical occupation probability p_q with $p_c < p_q \leq 1$ must exist, where extended wave functions appear for the first time for some part of the energy spectrum. The threshold p_q is known as quantum percolation threshold.

1.3.2
Vibrational Excitations and Oscillations

To model the propagation of virational excitations on networks we assume that equal masses M are placed on each node. Directly connected nodes n and $n + \delta$ are coupled by equal (scalar) force constants $D_{n,n+\delta}$. In this case, the components of displacements decouple, and we obtain the same equation of motion for all excitations $u_n(t)$,

$$M \, \frac{d^2}{dt^2} u_n(t) = {\sum_{\delta}}' \, D_{n,n+\delta} \left[u_{n+\delta}(t) - u_n(t) \right], \tag{1.12}$$

where again the sum runs over all k nodes $n + \delta$ having common edges with node n. The standard ansatz $u_n(t) = u_{n,\omega} \, \exp(-i\omega t)$ leads to the corresponding time independent vibration equation. Setting $M = D_{n,n+\delta} = 1$ (which determines the unit of the frequency) we obtain

$$\omega^2 \, u_{n,\omega} = {\sum_{\delta}}' \, (u_{n,\omega} - u_{n+\delta,\omega}), \tag{1.13}$$

which is an eigenvalue equation and has to be solved numerically by diagonalizing the dynamical matrix . Note that Eq. (1.13) is identical with Eq. (1.11) if we chose $t_{n+\delta,n} = -1$ for all neighboring nodes and $\epsilon_n = -\sum_\delta t_{n+\delta,n} = k_n$, where k_n is again the number of edges at node n.

For illustration, Fig. 1.4 shows representative vibrations of percolation clusters with varying occupation probabilities. One can observe a transition from the localized mode at the geometrical phase transition point $p = p_c$ towards more extended looking

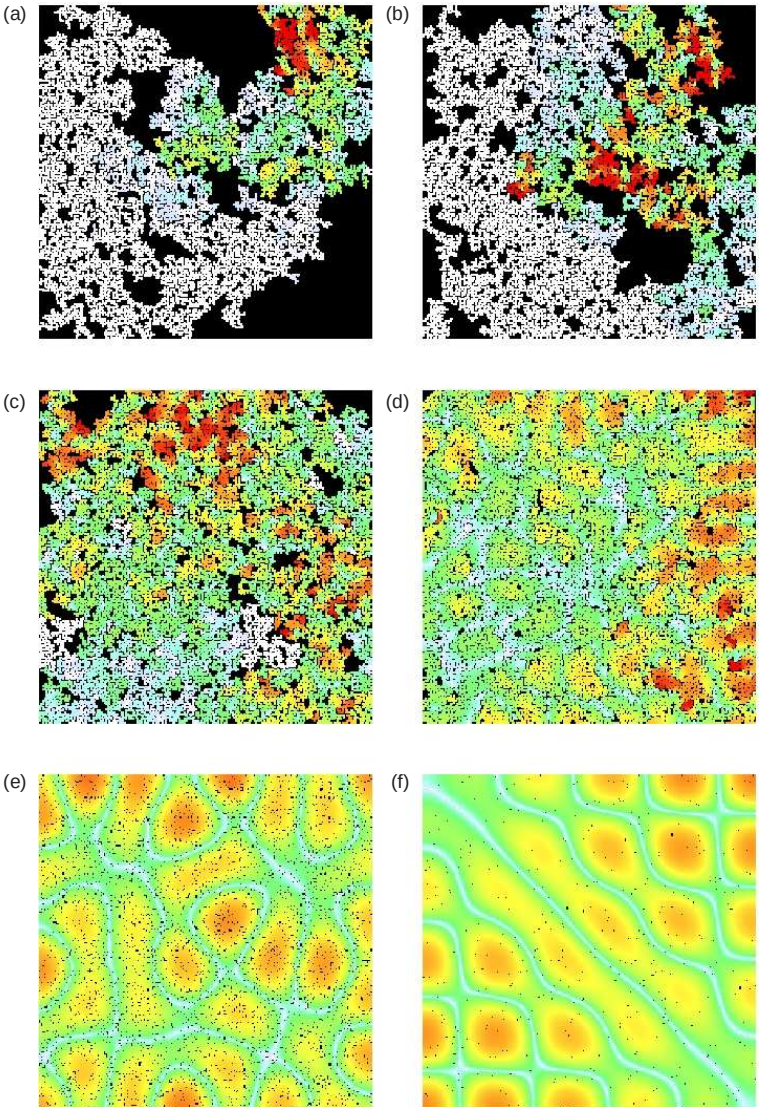

Fig. 1.4 Vibrational modes of percolation clusters on a square lattice at concentrations (a) $p = p_c$, (b) 0.61, (c) 0.65, (d) 0.75, (e) 0.90, and (f) 0.99. The black points are unoccupied sites and finite clusters. The vibrational amplitudes $|u_{n,\omega}|$ of the selected eigenmodes of Eq. (1.13) are color coded with red for maximum amplitude, followed by yellow, green and blue down to white for very small amplitudes. A transition from localized behavior at $p \approx p_c$ to extended-looking behavior for large p seems to occur. However, all modes are expected to be localized in the limit of infinite system size according to the single-parameter scaling theory [11] confirmed by numerical studies of level statistics [8]. Lattice size and frequency are 200×200 and $\omega^2 \approx 0.01 D/M$, respectively.

modes for larger values of p. Clearly, vibrational modes can be localized even if an infinite cluster exists. This is exactly the same as for electronic wave functions in quantum percolation. Anyway, electronic modes and vibrational modes are believed to be in the same universality class. The only difference regards the dispersion relation. For vibrations, the wave length diverges in the limit $\omega \to 0$, such that modes with very large wavelength always exist. By selecting a sufficiently large wavelength, one can always find a mode extending over the whole length of the system even if the occupation probability is arbitrarily close to the geometrical threshold p_c. There is thus no equivalent of the quantum percolation threshold p_q for vibrations. However, note that wavelength and correlation length of the modes are not identical [8].

Figure 1.4 also illustrates that looking at modes (eigenfunctions) may be misleading in studies of localization-delocalization transitions. None of the modes shown there is actually believed to be extended asymptotically (i. e., in the limit of infinite system size). This is a consequence of the universality of vibrational and electronic excitations and the singe-parameter scaling theory [11, 2], which excludes extended modes in dimensions $d \leq 2$. However, the modes shown in Fig. 1.4(e) and (f) look indeed extended, because their correlation lengths ξ are much larger than the considered lattice size. In particular for the largest value of p, $p = 0.99$ where just one percent of the sites is unoccupied, the mode is dominated by the boundary conditions and not much different from a common vibrational mode of a square plate with appropriately chosen frequency. The asymptotically localized nature of the vibrational modes on a two-dimensional lattice can be shown numerically by applying of level statistics (see Section 1.4) [8].

1.3.3
Optical Modes in a Network

A different perspective for the relevance of complex networks to real-world localization comes from considering optical networks. There is a long history of considering optical (or microwave) systems as a tool to analyze localization behavior. In 1982 Shapiro [47] has generalized a model proposed originally by Anderson *et al.* [48] to describe localization in disordered systems. Instead of a tight-binding description of a lattice (see Eq. (1.10)), Shapiro considered a model in which nodes are represented by beam splitters or cavities and edges by optical fibers or wave guides. From a theoretical point of view, this description is convenient since it yields a description the system in the scattering matrix formalism. This approach was taken a step further by Edrei *et al.* [49] who applied it to the dynamics of wave propagation (for example acoustic or light waves) in a disordered medium.

Such a description can form the basis of a real network built in a laboratory. For example a network of beam splitters and optical fibers may be constructed and its localization properties studied experimentally. Since optical fibers have a very low loss rate, there is no essential difference between connecting neighboring nodes or nodes far away from each other. Moreover, since in realistic optical set-ups the length of any optical fiber is much larger than the wave length of the light, the phase difference gained

by a wave as it transverses from one node to the next is always a fixed random number characteristic of this link (edge). Any form of a complex network (Cayley tree, random regular graph, Erdös-Rényi graph or scale-free network) can thus be constructed and studied on an optical bench. Although this seems experimentally feasible for small networks, to the best of our knowledge it has not been done. Furthermore, transitions in the transport properties of coherent waves on complex networks with long-range links might become relevant to typical real-world communication networks [27, 35]. Alternatively, one might consider a network of wave guides on the nanoscale similar to photonic lattices [5, 6].

Similar to the analogy between electronic and vibrational systems, the analogy between electronic and optical systems is quite general. The scalar wave equation is a good approximation for the propagation of an optical wave in an inhomogeneous medium as long as polarization effects are not important. It may be written as

$$\nabla^2\Psi + \frac{\epsilon(\vec{r})}{c^2}\frac{\partial^2}{\partial^2 t}\Psi = 0, \tag{1.14}$$

where $\epsilon(\vec{r}) = 1 + \delta\epsilon(\vec{r})$ describes the local fluctuations in the dielectric constant and c is the speed of light. Assuming a monochromatic wave, one may write $\Psi(\vec{r},t) = \psi(\vec{r})\exp(i\omega t)$, where ω is the frequency. Inserting $\Psi(\vec{r},t)$ into Eq. (1.14) yields

$$-\nabla^2\psi - \delta\epsilon(\vec{r})\psi = (\omega/c)^2\,\psi. \tag{1.15}$$

When this is compared with the stationary Schrödinger equation with a varying potential $U(\vec{r}) = U_0 + \delta U(\vec{r})$,

$$-\nabla^2\psi + \frac{2m}{\hbar^2}\delta U(\vec{r})\psi = \frac{2m}{\hbar^2}(E - U_0)\psi, \tag{1.16}$$

it can be seen that the Schrödinger equation and the scalar wave equation in random media are nearly identical up to constants. Thus, one may use techniques developed in the field of electronic localization in order to study the properties of optical networks.

Specifically for optical waves in a complex network of beam splitters and fibers, one can employ Eq. (1.11) with the coefficients $t_{n+\delta,n} = \exp(i\varphi_{n+\delta,n})$ for connected nodes and $t_{n+\delta,n} = 0$ for disconnected nodes. Here, $\varphi_{n+\delta,n}$ denotes the optical phase (modulo 2π) accumulated along the link. For simplicity, one can restrict $t_{n+\delta,n}$ to random values ± 1 to keep the Hamiltonian in the orthogonal symmetry class. The extension to unitary symmetry is straightforward. In this scenario, the on-site disorder W of the coefficients ϵ_n results from variations in the optical units (beam splitters) located at the nodes. Figure 1.1 shows the calculated intensities of three optical modes on complex networks with different clustering indices and no disorder in the beam splitters, $W = 0$.

1.3.4
Anderson Model with Magnetic Field

If an additional magnetic field is applied to electrons in a disordered solid, time-reversal invariance is broken, also yielding unitary symmetry. In the standard Anderson model

with additional magnetic field the critical disorder W_c is shifted to larger values [50, 51]. The phenomenological theory assumes that two length scales determine the behavior of the system. The first is the correlation (or localization) length as function of the disorder parameter, $\xi(W) \propto |W - W_c|^{-\nu}$. The second relevant length scale is the magnetic length given by $L_B = \sqrt{\hbar/eB}$, where B is the magnetic field. Rewriting the usual single-parameter scaling theory of the conductivity [11] with the ratio of these two length scales, Larkin and Khmel'nitskii [50] obtained

$$\sigma(B, W) \propto \frac{e^2}{\hbar L_B} \Phi \left(\left[\frac{L_B}{\xi(W)} \right]^{1/\nu} \right), \tag{1.17}$$

where $\Phi(x)$ is a scaling function equal to zero when x is of order of unity. The conductivity will thus be zero for $\xi \approx L_B$, or, using the definition of the correlation length, the field-dependent critical disorder $W_c(B)$ is related to $W_c(0)$ by $W_c(B) - W_c(0) \propto L_B^{-1/\nu} \propto B^{1/2\nu}$ for small B. Replacing the magnetic field B by the magnetic flux ϕ and inserting a constant factor W_ϕ yields a power-law behavior

$$W_c(\phi) - W_c(0) = W_\phi \phi^{\beta/\nu} \quad \text{with } \beta = 1/2. \tag{1.18}$$

In the Schrödinger Hamiltonian the magnetic field is introduced by substituting the momentum operator $\vec{p}$ with $\vec{p} - e\vec{A}$ [52]. In classical electrodynamics the vector potential is introduced as a convenient mathematical aid, but all fundamental equations are expressible in terms of fields. This is no longer true in quantum mechanics, where $\vec{A}$ is necessary to introduce the magnetic field. Therefore, $\vec{A}$ is relevant for quantum objects, even if $\vec{B} = \vec{\nabla} \times \vec{A}$ is zero.

Here we chose Landau gauge for the vector potential, $\vec{A} = B(0, x, 0)$, to simplify the problem. Therefore, the (non-diagonal) hopping matrix elements of the tight-binding Hamiltonian (1.10) with $\vec{R}_{n+\delta} = \vec{R}_n \pm \vec{e}_y$ read $t_{n+\delta,n} = t \exp(\pm 2\pi i \phi_{n+\delta,n} m)$ where $m = \vec{R}_n \cdot \vec{e}_x$, and $\phi_{n+\delta,n} = \varphi_{n+\delta,n}/\varphi_0$ is the ratio of flux $\varphi_{n+\delta,n} = a^2 B_{n+\delta,n}$ through a lattice cell with size a^2 to one flux quantum $\varphi_0 = h/e$. For bonds in the x or z direction the non-diagonal matrix elements are $t_{n+\delta,n} = t$. The results for $\phi_{n+\delta,n} = \epsilon$ and $\phi_{n+\delta,n} = 1/4 + \epsilon$ are invariant under the shift $\epsilon \to -\epsilon$. The range $\phi_{n+\delta,n} = 0$ to $\phi_{n+\delta,n} = 1/4$ thus represents the full flux spectrum from the flux free case to the largest possible flux.

A constant magnetic field is described by constant flux $\phi_{n+\delta,n} = \phi$ through each plaquete. On the other hand, a spatially random magnetic flux is described by random phases $\phi_{n+\delta,n}$ such that the $t_{n+\delta,n}$ are random complex numbers with absolute value t. Note that this is the only option for a complex network where there is no real space and directions are arbitrary. Since hopping terms of the form $t_{n+\delta,n} = \exp(i\varphi_{n+\delta,n})$ (i. e., with $t = 1$) also occur for optical networks, the Anderson model with random magnetic fields is equivalent to this case.

1.4 Level Statistics

Next we describe the technique of level statistics that can be used to study localization-delocalization transitions of the modes in all four models introduced in the previous section by analyzing eigenvalues instead of eigenfunctions.

1.4.1 Random Matrix Theory

Level statistics was first used in nuclear physics [53] to understand complex excitation spectra of heavy nuclei. It is not feasible to calculate the energy spectra distribution using elementary quantum physics, but a qualitative description using random matrix theory [54] succeeded. In the eighties random matrix theory was introduced in solid state physics to understand the chaotic eigenvalue spectra of disordered solid systems [55, 56]. The connections to metal-insulator transitions were realized a few years later, and level statistical methods were then used for numerical investigations of the Anderson transition [57, 58, 59], see [60, 61, 62] for review articles.

In random matrix theory one studies 2×2 matrices, with random numbers as matrix elements $A_{n,m}$. In the case of Gaussian orthogonal ensembles (GOE) the matrix elements $A_{1,1}$, $A_{1,2} = A_{2,1}$ and $A_{2,2}$ can be transformed by orthogonal transformations. Using infinitesimal transformation techniques, the diagonal matrix elements can be shown to be Gaussian distributed with mean E_0 and standard deviation σ, while the non-diagonal elements have zero mean and standard deviation $\sigma/\sqrt{2}$. After calculating the two eigenvalues A_1 and A_2 of the random matrices one determines their normalized distances $s = |A_1 - A_2|/(\sqrt{\pi}\sigma)$ with $\langle s \rangle = 1$. The distribution of these level spacings s follows the parameter-free Wigner distribution

$$P_{\mathrm{GOE}}(s) = \frac{\pi}{2} s \exp\left[-\frac{\pi}{4} s^2\right]. \tag{1.19}$$

Because $P_{\mathrm{GOE}}(s) \to 0$ for $s \to 0$, the probability of degenerated or similar eigenvalues is zero or suppressed; this is known as eigenvalue repulsion. For large level spacings the Wigner distribution has a Gaussian tail.

Hermitian matrices with complex random matrix elements and invariance under unitary transformations represent the Gaussian unitary ensemble (GUE). In this case the Wigner distribution of the normalized level spacings s is similar to Eq. (1.19),

$$P_{\mathrm{GUE}}(s) = \frac{32}{\pi^2} s^2 \exp\left[-\frac{4}{\pi} s^2\right]. \tag{1.20}$$

If also rotational symmetry is broken, we obtain the Gaussian symplectic ensemble (GSE). The corresponding distribution $P_{\mathrm{GSE}}(s)$ shows even stronger level repulsion, increasing as $P_{\mathrm{GSE}}(s) \propto s^4$ for small s.

Although they are exact only for 2×2 matrices, $P_{\mathrm{GOE}}(s)$, $P_{\mathrm{GUE}}(s)$, and $P_{\mathrm{GSE}}(s)$ are a good approximations for level-spacing distributions of large random matrices with the corresponding symmetry. Extensive numerical investigation have shown that this

holds even for sparsely filled matrices. Consequently, the level spacing distributions of the tight-binding Hamiltonian (1.10) can be described by random matrix theory.

1.4.2 Level Statistics for Disordered Systems

There are two cases for which the Wigner distributions given in the previous subsection are not correct. (i) The matrices are not random, i. e. not disordered. The eigenvalue of ordered or nearly ordered systems are nearly equidistant and some are degenerated. Therefore, they cannot be repulsive. (ii) The eigenstates are localized. In this case the eigenfunctions do not overlap and the eigenvalues are therefore independent. The level spacings of independent eigenvalues (or the spacings between random numbers in general) are characterized by a Poisson distribution

$$P_{\mathrm{P}}(s) = \exp[-s]. \tag{1.21}$$

In this case, the levels do not repel and degeneration is probable, $P_{\mathrm{P}}(0) = 1$. The tail of the Poisson distribution is a simple exponential, decreasing much slower than the Wigner distributions (1.19) and (1.20).

Consequently, level-spacing distributions of tight-binding Hamiltonians can be used for determining metal-insulator transitions [57, 58, 59]. The distributions $P_{\mathrm{P}}(s)$ for localized states and $P_{\mathrm{GOE}}(s)$ or $P_{\mathrm{GUE}}(s)$ for extended states are valid asymptotically in the limit of infinite system size. For finite systems, the numerical $P(s)$ is intermediate, approaching the limiting distributions for increasing system sizes, since finite-size corrections (for example due to boundary conditions) become smaller with increasing system size. Therefore, the numerical $P(s)$ changes towards a Poisson distribution, if eigenfunctions are localized. And it changes towards a Wigner distribution, if they are extended. Only at the transition point (the critical disorder) the numerical $P(s)$ is system-size independent. However, the exact form of the critical distribution $P_c(s)$ cannot be determined analytically. It depends on the topology of the system and even boundary conditions.

Figure 1.5 shows the numerical level-spacing distributions $P(s)$ for optical modes on large scale-free networks without diagonal disorder ($W = 0$) and varied clustering index C_0 (see Fig. 1.1 for pictures of the structures and the modes; see Section 1.2.2 for clustering in complex networks). The two limiting cases $P_{\mathrm{GOE}}(s)$ [Eq. (1.19)] and $P_{\mathrm{P}}(s)$ [Eq. (1.21)] are plotted for comparison. One can clearly see that the shape of the numerical $P(s)$ changes from Wigner to Poisson with increasing C_0. The same type of plot is found when studying a localization-delocalization transition in the standard Anderson model by considering a normal lattice and increasing the diagonal disorder strength W from $W < W_c$ to $W > W_c$. Clustering in complex networks can thus cause an Anderson-like localization-delocalization transition although there are no on-node disorder W and no changes in the degree distribution $P(k)$.

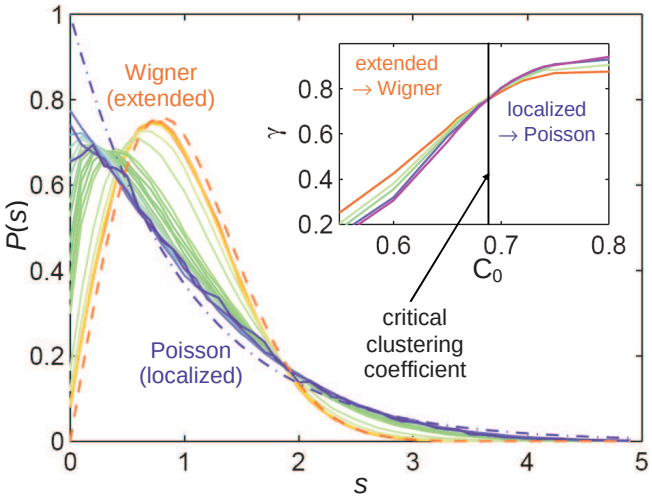

Fig. 1.5 Level-spacing distribution $P(s)$ for optical modes on scale-free networks with degree-distribution exponent $\lambda = 5$, system size $N = 12500$ and no disorder, $W = 0$. A clear transition from Wigner (dashed red curve) to Poisson (dash-dotted blue curve) behavior is observed as a function of the clustering coefficient prefactor C_0 increasing from $C_0 = 0.0$ (continuous red curve) to $C_0 = 0.90$ (continuous blue curve). Inset: localization parameter γ [see Eq. (1.22)] versus C_0 for networks with $N = 5000$ (red), $N = 7500$ (light green), $N = 10000$ (green) , $N = 12500$ (blue), and $N = 15000$ (purple). A transition from extended modes for small C_0 to localized modes for large C_0 is observed at $C_{0,q} \approx 0.69$. The results are based on eigenvalues around $|E| = 0.2$ and 0.5. Figure adapted from [22].

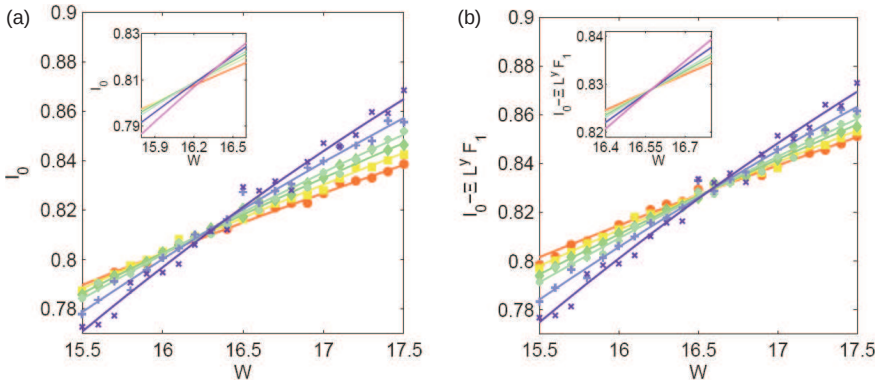

Fig. 1.6 The localization parameter $I_0 = \langle s^2 \rangle / 2$ versus disorder W for the standard three-dimensional Anderson model with linear sizes $L = 14$ (red circles), 17 (yellow squares), 20 (green diamonds), 23 (light blue stars), 30 (blue pluses), and 40 (pink crosses) and hard-wall boundary conditions. The lines correspond to fits of Eq. (1.29). Insets: the region around the crossing point zoomed in. In (b) the I_0 values are corrected by subtraction of the irrelevant scaling variables.

The actual transition point can be determined more accurately by analyzing the system-size (L) dependence of [58]

$$\gamma(L) = \frac{\int_2^\infty P(s)ds - \int_2^\infty P_{\rm GOE}(s)ds}{\int_2^\infty P_{\rm P}(s)ds - \int_2^\infty P_{\rm GOE}(s)ds}, \tag{1.22}$$

where $\gamma \to 0$ if $P(s)$ approaches the Wigner distribution, and $\gamma \to 1$ if it approaches the Poisson distribution. The inset of Fig. 1.5 shows γ for five system sizes versus the clustering strength C_0. Indeed, γ decreases with system size for small values of C_0 while it increases with size for large values of C_0. One can thus observe the phase transition at the critical value $C_{0,q} \approx 0.69$ by the crossing of the five curves, indicating a system-size independent critical value of $\gamma_c \approx 0.76$.

Alternatively the full level-spacing distribution $P(s)$ can be parametrized by its second moment,

$$I_0(L) = \frac{1}{2}\langle s^2 \rangle = \frac{1}{2}\int_0^\infty s^2 P(s)ds, \tag{1.23}$$

which converges to 1 for localized modes (Poisson limit) and to 0.637 or 0.589 for extended modes (GOE or GUE Wigner limit, respectively). Figure 1.6 exemplifies the determination of W_c for the metal-insulator transition based on I_0 for different system sizes and different W in the standard three-dimensional Anderson model with diagonal disorder and hard-wall boundary conditions.

1.4.3
Corrected Finite-Size Scaling

In some cases, finite-size effects can become rather strong, so that there is no unique crossing point of the γ or I_0 curves for different system sizes L. One example is shown in Fig. 1.6(a), see magnification of the crossing region in the inset. In such cases, the effects of irrelevant scaling variables must be subtracted [46].

To describe the procedure, we assume that a parameter Γ characterizing the localization properties will depend only on the ratio of the linear system size L and the characteristic (correlation) length scale $\xi \sim |W - W_c|^{-\nu}$,

$$\Gamma(L, W) = F[L/\xi(W)]. \tag{1.24}$$

Here, Γ can stand for either γ or I_0 introduced in the previous section, while W represents any parameter characterizing the disorder. In particular, W might be replaced by C_0 if effects of clustering rather than diagonal disorder are considered or by p if effects of percolation are considered. Although $\Gamma(L, W)$ is a non-continuous function of W for $L = \infty$, it is analytical for finite L and thus F can be expanded around the critical point, $F(x) = a + bx^{1/\nu} + cx^{2/\nu} + \ldots (x \to 0)$, leading to

$$\Gamma(L, W) \approx \Gamma(L, W_c) + R|W - W_c|L^{1/\nu} \tag{1.25}$$

with constant R. Here, irrelevant scaling variables Ξ, decaying with the system size L are not included. Hence the scaling formula (1.24) has to be extended to include relevant Υ and irrelevant Ξ scaling variables,

$$\Gamma = F(\Upsilon L^{1/\nu}, \Xi L^y). \tag{1.26}$$

If irrelevant scaling variables do not introduce discontinuities, F is expandable not only around the relevant scaling variable Υ up to order n_R, but also around the irrelevant scaling variable Ξ up to order n_I,

$$\Gamma = \sum_{n=0}^{n_R} \Upsilon^n L^{n/\nu} F_n(\Xi L^y) \quad \text{with} \quad F_n(\Xi L^y) = \sum_{m=0}^{n_I} \Xi^m L^{my} F_{nm}. \tag{1.27}$$

The scaling variables are analytical functions of the dimensionless disorder $w = (W_c - W)/W_c$ and therefore equally expandable,

$$\Upsilon(w) = \sum_{n=1}^{m_R} b_n w^n \quad \text{and} \quad \Xi(w) = \sum_{n=0}^{m_I} c_n w^n, \tag{1.28}$$

up to order m_R for the relevant and m_I for the irrelevant variables, respectively. The relevant scaling variable vanishes at criticality, thus, $b_0 = 0$, whereas c_0 is finite, introducing a size-dependent error. A size-independent Γ_c at criticality is reestablished by subtracting the terms with irrelevant variables. The absolute scales of the arguments are unknown. However, they can be fixed by choosing e. g., $F_{01} = F_{10} = 1$ in Eq. (1.27). The total number of fitting parameters is thus $N_p = (n_I + 1)(n_R + 1) + m_R + m_I + 2$.

Figure 1.6 depicts a typical example for the three-dimensional Anderson model with hard-wall boundary conditions. I_0 is expanded up to orders $n_I = 1$, $n_R = 3$, $m_R = 1$ and $m_I = 0$ such that

$$I_0(W, L) = F_0(\Upsilon L^{1/\nu}) + \Xi L^y F_1(\Upsilon L^{1/\nu}). \tag{1.29}$$

In Fig. 1.6(a) I_0 is shown without the corrections. No well definable crossing point exists, i. e., I_0 is still L dependent at criticality. In Fig. 1.6(b) the corrected quantity $I_0 - \Xi L^y F_1$ is shown. The lines cross at one well defined point as seen in the inset. The critical disorder for the three-dimensional Anderson model with hard-wall boundary conditions is given by $W_c = 16.57 \pm 0.13$ in agreement with the most recent numerical result $W_c = 16.54$ [46]. For periodic boundary conditions the effect of the irrelevant scaling variables is negligible.

1.4.4
Finite-Size Scaling with Two Parameters

To analyze the localization-delocalization transition for networks with clustering (characterized by C_0) *and* on-node disorder W the finite-size scaling equations have to be extended such that two parameters can be taken into account simultaneously. Without considering irrelevant variables this yields

$$\Gamma(C_0, W, L) = \Gamma_c + [R_1|C_0 - C_{0,q}| + R_2|W - W_c|]\, L^{1/\nu}, \tag{1.30}$$

where R_1 and R_2 are constants. Using Eq. (1.30) one can determine the coordinates $C_{0,q}$ and W_c of the localization-delocalization-transition point for scale-free networks with various λ. A corresponding plot involving just data with varying C_0 is shown in Fig. 1.7.

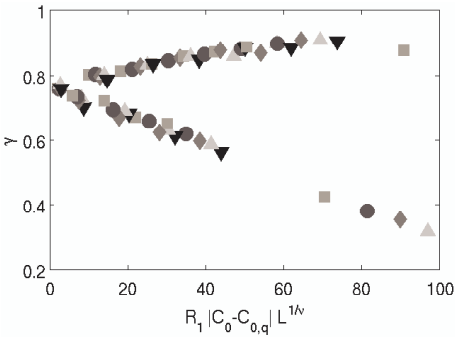

Fig. 1.7 Finite-size scaling of γ according to Eq. (1.30) for optical modes on scale-free networks with $\lambda = 5$ (like in Fig. 1.5), without on-node disorder, $W = 0$. The considered system sizes are $N = 5,000$ (squares), $7,500$ (circles), $10,000$ (diamonds), $12,500$ (triangles up), and $15,000$ triangles down. The two branches correspond to the extended regime (bottom) and localized regime (top).

The system size of the considered scale-free networks has to be approximated by $L \propto \ln(a(C_0)N)$, where the N dependence is well established [28] but the C_0 dependence hardly explored. Our data for N up to 10^5 suggested $\ln a \propto (C_0 - C_{0,c})^{-\nu_c}$, where $C_{0,c}$ denotes the classical transition point where the whole network breaks into pieces by strong clustering, and the giant component ceases to exist. Since $C_{0,q} < C_{0,c}$, a and thus L depend weakly on C_0 at the wave localization transition point.

1.5
Localization-Delocalization Transitions in Complex Networks

In this Section we review numerical results for localization-delocalization transitions in complex networks determined by means of level statistics. Anderson and quantum percolation transitions, which seem to be in the same universality class, have been studied on different topologies including quasi-fractal structures [63], percolation networks [64, 65, 66, 67, 68, 69, 70, 71, 72], Cayley trees [20], and small-world networks [21]. Transitions of vibrational modes were also studied on percolation networks [8]. In all these cases, the transitions were induced either by on-site disorder or by cutting bonds (percolation) and thus by changing the degree distribution of the network. Furthermore, quantum phase transitions (and also classical phase transitions) induced by mere topological changes of the network, i. e., changes in the clustering index, have been found recently [22] even with zero on-site disorder.

1.5.1
Percolation Networks

For quantum percolation on a quadratic lattice it is believed, but not undisputed [64, 66], that all eigenfunctions are localized ($p_q = 1$) [65, 67, 69] as predicted by the single-parameter scaling theory [11]. All studies based on level statistics find no extended states in two-dimensional systems. For quantum percolation on a simple cubic lattice the critical occupation probability $p_q \approx 0.44 > p_c \approx 0.312$ for site percolation [68, 71] and $p_q^b \approx 0.33 > p_c^b \approx 0.247$ for bond percolation [68, 70] are reported; the study

network	$\langle k \rangle$	l	W_c	ν
scale-free, $\lambda = 4$, $m = 2$	2.97	12.46	15.7±0.9	0.55±0.11
random-regular	3	11.8	11.9±0.26	0.66±0.08
Erdös-Rényi	3	9.45	20.5±0.23	0.68±0.08

Table 1.2 Small-world networks showing a transition from localized to extended states. The number of nodes on the last shell l is reported for networks of size $N = 1000$. The critical disorder W_c and the critical exponent ν have been determined by level statistics. Data taken from [21].

by Berkovits *et al.* [70] being based on level statistics. The values for the critical exponent ν are similar to the Anderson transition: $\nu \approx 1.35$ [70], and $\nu \approx 1.46$ [72]. This is expected, because the Anderson model and quantum percolation are in the same universality class.

The localization behavior of vibrational modes of infinite site percolation clusters above the critical concentration has been studied in two and three dimensions using level statistics [8]. While all eigenstates are localized in $d = 2$, clear evidence for a localization-delocalization transition was found in $d = 3$. However, contrary to the common view this transition occurs for frequencies above the phonon-fracton crossover and gives rise to a regime of extended fracton states. The term 'fracton' is used for virational modes of a fractal structure [74], if the wavelength $\lambda \sim \omega^{-2/d_w}$ of a mode with frequency ω is smaller than the correlation length $\xi_p(p) \sim |p - p_c|^{-\nu_p}$ of the percolation structure. In these equations, ν_p denotes the critical exponent of percolation ($\nu_p = 4/3$ in $d = 2$ and 0.875 in $d = 3$), while d_w is the random walk exponent ($d_w = 2.88$ in $d = 2$ and 3.8 in $d = 3$). In the fracton regime, the density of states is characterized by $g(\omega) \sim \omega^{d_s - 1}$ with the spectral dimension $d_s = 2d_f/d_w \approx 4/3$ (and d_f the fractal dimension) [74] rather than $d_s = d$ for non-fractal structures. It was found that the crossover from the fracton regime to a standard phonon regime ($\lambda \sim \omega^{-1}$, $g \sim \omega^{d-1}$) occurs independent of the localization-delocalization transition [8]. In $d = 2$ there is only the fracton-phonon crossover and all modes are asymptotically localized for non-zero disorder. In $d = 3$ the crossover occurs at frequencies which are larger than those for the localization-delocalization transition by approximately a factor of three [8].

1.5.2
Small-World Networks without Clustering

The localization behavior of electrons in random networks, Erdös-Rényi networks, and scale-free networks without clustering was studied using level statistics [21]. A clear localization-delocalization transition at particular strengths W_c of the on-node disorder has been observed for a group of networks, which are all characterized by an average degree $\langle k \rangle \leq 3.1$ and an averaged size of the last occupied shell $l \geq 9.45$. The results are summarized in Table 1.2.

For several other small-world networks with $\langle k \rangle \geq 3.1$ no transition towards localized electronic eigenfunctions could be observed [21]. Nevertheless, one should be rather careful in interpreting this observation since larger values of $\langle k \rangle$ lead to smaller sizes l of the network for the same number of nodes N.

The data for all the networks (including those which show no clear signs of transition) can be scaled according to their average degree $\langle k \rangle$. The larger the value of $\langle k \rangle$, the larger is also the value of W needed to obtain a specific value of γ [see Eq. (1.22)]. For all the small-world networks showing a localization-delocalization transition, the critical exponent ν is approximately equal to $1/2$. A critical index of $\nu = 1/2$ is expected for a system of infinite dimensionality [15, 63].

The main features of the Anderson transition are thus similar for a wide range of small-world networks. However, the fact that networks with high connectivity are very compact raises the problem of identifying the transition point. It is hard to extend the usual finite-size scaling method to networks with high connectivity since the number of sites grows very rapidly with size, while for small network sizes the crossover behavior of the γ curves is very noisy. This results in an inability to clearly identify the Anderson transition for scale-free networks with $\langle k \rangle \geq 3.1$. The possibility of a critical connectivity above which no transition exists cannot be ruled out.

1.5.3
Scale-Free Networks with Clustering

In a recent paper [22] we have studied the localization-delocalization transition for optical modes on scale-free networks with clustering. By exact diagonalization, we have calculated the eigenvalues of Eq. (1.11) with random hopping elements $t_{n,m} = \pm 1$ characterizing the links between all connected nodes. The networks are characterized by the exponent λ in the scale-free degree distribution Eq. (1.2), the clustering coefficient prefactor C_0 from Eq. (1.5) as well as the strength of the on-node disorder W. We applied level statistics to determine the localization behavior of the modes and to extract the phase-transition points.

Figure 1.8(a) shows the phase diagram for the transition from localized (upper right) to extended (lower left) optical modes. The horizontal axis ($C_0 = 0$) corresponds to the case without clustering described in the previous section. Here, the critical disorder W_c depends on λ. The main result regards the transitions on the vertical axis. Without on-node disorder (for $W = 0$), the transition to a localized phase occurs at a critical clustering $C_{0,q}$ that depends on λ, i. e., the degree distribution. While even the strongest clustering $C_0 = 1$ cannot achieve such a transition if $\lambda < 4$, values of $C_{0,q} < 1$ are observed for $\lambda > 4$. The case $\lambda = 4$ seems to be limiting, since it represents the broadest degree distribution allowing for a localization-delocalization phase transition upon increasing clustering.

If variations of C_0 *and* W are considered, the full phase diagram can be explored. Evidently, smaller values of C_0 are sufficient for localization-delocalization phase transitions if $W > 0$. Within our error bars the critical exponent ν corresponds to the mean-field value $\nu = 1/2$ for infinite dimensions. This is shown in Fig. 1.8(b) and

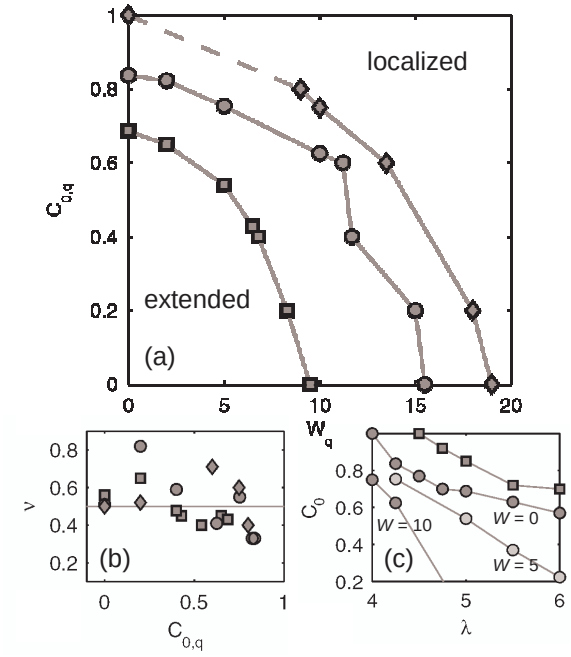

Fig. 1.8 (a) Phase diagram for transitions from localized optical modes (upper right) to extended modes in parts of the spectrum (lower left) for different degree distribution exponents $\lambda = 4$ (diamonds), 4.25 (circles), and 5 (squares). (b) Critical exponent ν for different λ and $C_{0,q}$. The values are consistent with the mean-field prediction $\nu = 1/2$. (c) Quantum transitions (circles) and classical transitions (squares) as a function of the degree exponent λ. In the regime $\lambda < 4.5$ only quantum transitions occur. For $W > 0$ the curves move downwards making quantum transitions possible for $\lambda < 4$. Figure redrawn from [22].

expected for an Anderson-type transition [15]. We obtained similar phase diagrams for networks with homogeneous or Erdös-Renyi-type degree distributions (not shown).

There are several similarities between the phase transitions induced by clustering and by quantum percolation. In both cases the giant component becomes smaller when the parameters C_0 and p approach the quantum transition points $C_{0,q}$ and p_q, respectively; the extended phase exists for $C_0 < C_{0,q}$ and for $p > p_q$. One also finds a geometrical phase transition after the quantum phase transition in both cases, since the network breaks for $C_0 > C_{0,c}$ and $p < p_c$. In between, there is a regime with a giant component (or an infinite cluster) but merely localized modes for $C_{0,q} < C_0 < C_{0,c}$ and $p_c < p < p_q$. However, the relation between both types of transitions is still an open question. The changes in the degree distribution of the giant component are not sufficient to explain the classical transition.

To make sure that the quantum transition is induced by clustering and not by a classical phase transition we have determined the corresponding classical critical clustering coefficient $C_{0,c}$. For this purpose we have analyzed the size N_2 of the second largest cluster in the system which should increase with C_0 if the giant component exists ($C_0 < C_{0,c}$) and decrease for higher values of C_0 if it broke down ($C_0 > C_{0,c}$) [26, 40]. We found no indications of a classical transition for $\lambda < 4.5$, i. e. the giant component is not broken. For $\lambda = 5$ we found $C_{0,c} \approx 0.85$, significantly larger than $C_{0,q} \approx 0.69$ as shown in the inset of Fig. 1.5 and in Fig. 1.8(c).

The localization-delocalization transition for $W = 0$ is thus clearly different from the classical one in two ways. (i) There is no classical transition for $\lambda < 4.5$ although a quantum transition is clearly seen. (ii) For $\lambda > 4.5$, the quantum transition occurs

ϕ	0.0	0.0008	0.0015	0.004	0.007	0.01	0.03	0.1	0.25
W_c	16.54	17.09	17.21	17.44	17.16	17.27	17.65	18.16	18.14

Table 1.3 Fitting results for the critical disorder W_c in the three-dimensional Anderson model with magnetic flux ϕ. Error bars of the combined fits between ± 0.03 and ± 0.08 have been calculated with the bootstrap method. $\phi = 0.0008$ is the lowest nonzero flux that could be studied in the considered system sizes (up to 40^3 lattice points), since at least one whole flux quantum must penetrate the system.

for lower C_0 values than the classical one, leaving an intermediate regime ($C_{0,q} < C_0 < C_{0,c} \leq 1$) in which all modes are localized although there is a spanning giant cluster. Clustering represents a new degree of freedom that can be used to induce and study phase transitions in complex networks. Comparing systems with different clustering properties might enable one to find the most relevant cause of quantum localization. We proposed that the phenomenon should be observable experimentally and relevant in complex coherent optical networks made of fibers and beam splitters. Such experiments would directly probe the influence of complex network topology on the Anderson localization of light [3, 4, 6, 5].

1.5.4
Systems with Constant and Random Magnetic Field

Finally, we want to look at the Anderson model with additional magnetic field. As described in Section 1.3.4 the field destroys time reversal invariance and leads to complex values of the hopping terms $t_{n+\delta,n}$ in the eigenvalue equation (1.11). The model with random magnetic flux is thus equivalent with the full description of an optical network with the complete range of phase shifts for light propagation along the links (see also Section 1.3.3).

For the Anderson localization-delocalization transition on a standard three-dimensional lattice with a constant magnetic field B a systematic increase of the critical disorder W_c with magnetic flux ϕ was predicted by Larkin and Khmel'nitskii already in 1981 [50], see Eq. (1.18). The prediction was verified in several different sophisticated analytical studies. Numerical work, however, concentrated on the effect of large or random magnetic fluxes [75, 76].

Very recently, this prediction was confirmed for small values of ϕ by extended numerical simulations based on level statistics [51]. Note that the Anderson model with hard-wall boundary conditions must be used in this case, since it is not possible to match the increases of the magnetic vector potential with periodic boundary conditions unless very large systems or very large fluxes are considered. The disadvantage, however, is that irrelevant scaling variables must be taken into account explicitly in the corrected finite-size scaling approach (see Section 1.4.3).

Table 1.3 shows preliminary numerical results for the critical disorder strengths $W_c(\phi)$, which are indeed increasing with magnetic flux ϕ. The increase is very strong

network	p_c^b	$p_q^b(\phi = 0)$	$p_q^b(\phi > 0)$
simple cubic lattice	0.247	0.325	0.313
random regular network, $k_0 = 6$	0.200	0.237	0.239
random regular network, $k_0 = 4$	0.333	0.398	0.395
Erdös-Rényi network, $k_0 = 4$	0.250	0.327	0.323

Table 1.4 Classical percolation thresholds p_c^b for bond percolation on different networks and preliminary results for the corresponding quantum bond percolation thresholds p_q^b without and with magnetic flux ϕ. The error bars of the p_q values are at least 0.01. Therefore, no significant effect of the magnetic field on the quantum percolation thresholds is observed.

already for weak fluxes, the prefactor W_ϕ in Eq. (1.18) being surprisingly large for both, small and large ϕ: $W_\phi = 4.9 \pm 0.4$ and 3.8 ± 0.1, respectively. This type of behavior naturally leads to the idea that the effect might be used as the basis of a very sensitive low-temperature sensor for magnetic flux. In addition, the data can be fit by Eq. (1.18) with exponents $\beta = 0.45 \pm 0.05$ and 0.60 ± 0.07 for small and large ϕ, respectively. The prediction of Larkin and Khmel'nitskii is thus confirmed also regarding the scaling exponent $\beta = 1/2$. The reason for dividing the fit into two regions for small and large ϕ stems from a slight shift in the critical level spacing distribution $P_c(s)$.

For strong random magnetic fields an even larger critical disorder strength $W_c = 18.80$ has been reported [76] based on calculations with the transfer matrix method. We can thus conclude that a constant and a random magnetic field lead to a significant shift of the localization-delocalization transition in systems on regular lattices.

However, preliminary results show that this is not the case for quantum percolation transitions and for localization-delocalization transitions on complex networks. Table 1.4 compares the classical percolation thresholds with the quantum percolation thresholds without and with random magnetic field. Note that a constant magnetic field is not an option for complex networks; however, the effect of magnetic fields was strongest for the random field in the Anderson model on a lattice. One can clearly see that the magnetic field (and the corresponding change from orthogonal to unitary symmetry) have no significant effect on the quantum localization-delocalization transition.

1.6 Conclusion

In summary, we have shown that localization-delocalization transitions (Anderson transitions) of electronic, vibrational, and optical modes occur in disordered systems because of backscattering and interference on time-reversed paths. The disorder can be due to a random potential landscape on a lattice (standard Anderson model) or to a complex structure of the network describing the system. Focusing on the latter case, we have shown that the localization-delocalization transition of percolation systems

(i. e., quantum percolation) can be well distinguished from the classical (geometrical) percolation transition. On even more complex networks characterized by a small distance between all nodes (small-world property), a scale-free degree distribution, and clustering (increased probability of fully connected triangles) the same type of wave localization transition is observed. It is also clearly distinct from the classical percolation transition occurring in complex networks upon cutting edges (links). We have shown that changing only the local structure of a scale-free network by increasing the clustering coefficient can drive a localization-delocalization transition, even if there is no on-node disorder and no edges are cut.

The numerical technique used in most of the reviewed studies is level statistics together with finite-size scaling. This approach can characterize the localization properties of eigenfunctions of the considered Hamiltonian or dynamical matrix without actually requiring the calculation of the eigenfunctions. Making use of random matrix theory, it is based on studying the distribution of normalized level spacings obtained from eigenvalues only. This is a significant advantage for the computational effort, and it allows considering much larger systems. In particular in systems with hard-wall boundary conditions, the finite-size scaling approach has to be supplemented by taking into account irrelevant scaling variables.

The nature of the considered wave-like excitations is not essential for the transitions, since the wave character can be due to quantum theory (electrons) or just classical mechanics (vibrational modes). Similar phenomena can be expected for spin waves in disordered solids, which yield the same type of eigenvalue equation. Studying the localization of light waves is also equivalent in theory. However, it is more complicated experimentally on the one hand, since localization effects can hardly be distinguished from absorption effects. On the other hand, laser light has a macroscopic coherence length. Studying localization effects in complex networks of fibers and beam splitters might thus become experimentally feasible on an optical table. Such experiments could directly probe the influence of complex network topology on the Anderson localization of light [3, 4, 5, 6].

We have also considered electronic systems with additional random and non-random magnetic field. Introducing the magnetic fields changes the universality class of the Hamiltonian from orthogonal to unitary. The case with strong random magnetic field is equivalent with the full description of an optical network, in which random phase shifts occur for light waves traveling through fibers (edges) between beam splitters. We showed that a constant magnetic field has a significant effect on the critical disorder characterizing the localization-delocalization transition (metal-insulator transition) on a lattice and confirmed a predicted scaling law down to very low fields. On a lattice, also random fields have a strong effect.

However, this does not hold for localization-delocalization transitions in complex networks like percolation networks or small-world networks. Complex networks are characterized by strong topological disorder rather than on-node potential disorder. In this case, the symmetry class of the Hamiltonian (or the dynamical matrix) seems to be much less important. Therefore, if the non-zero non-diagonal terms are already distributed in a strongly disordered fashion in the matrix due to the disordered topological structure, the actual range of the values and even the type (real or complex) does not

matter much. Hence, the properties of light modes, vibrational modes and electronic modes on complex networks are even more similar than they are on regular lattices with on-site disorder.

Acknowledgement

We would like to thank Prof. Shlomo Havlin for discussions. The work has been supported by the German Research Foundation (DFG), the European Community (grant 231288, project SOCIONICAL), the Minerva Foundation, the Israel Science Foundation (grant 569/07 and National Center for Networks), and the Israel Center for Complexity Science.

References

1 Anderson, P.W.: Absence of Diffusion in Certain Random Lattices. Phys. Rev. **109**, 1492–1505 (1958)

2 Kramer, B., MacKinnon, A.: Localization – Theory and Experiment. Rep. Prog. Phys. **56**, 1496–1564 (1993)

3 Wiersma, D.S., Bartolini, P., Lagendijk, A., Righini, R.: Localization of Light in Disordered Medium. Nature **390**, 671–673 (1997)

4 Störzer, M., Gross, P., Aegerter, C.M., Maret, G.: Observation of the Critical Regime Near Anderson Localization of Light. Phys. Rev. Lett. **96**, 063904 (2006)

5 Schwartz, T., Bartal, G., Fishman, S., Segev, M.: Transport and Anderson Localization in Disordered Two-Dimensional Photonic Lattices. Nature **446**, 52–55 (2007)

6 Lahini, Y., Avidan, A., Pozzi, F., Sorel, M., Morandotti, R., Christodoulides, D.N., Silberberg, Y.: Anderson Localization and Nonlinearity in One-Dimensional Disordered Photonic Lattices. Phys. Rev. Lett. **100**, 013906 (2008)

7 Foret, M., Courtens, E., Vacher, R., Suck, J.B.: Scattering Investigation of Acoustic Localization in Fused Silica. Phys. Rev. Lett. **77**, 3831–3834 (1996)

8 Kantelhardt, J. W., Bunde, A., Schweitzer, L.: Extended Fractons and Localized Phonons on Percolation Clusters. Phys. Rev. Lett. **81**, 4907–4910 (1998)

9 Billy, J., Josse, V., Zuo, Z.C., Bernard, A., Hambrecht, B., Lugan, P., Clement, D., Sanchez-Palencia, L., Bouyer, P., Aspect, A.: Direct Observation of Anderson localization of Matter Waves in a Controlled Disorder. Nature **453**, 891 (2008)

10 Roati, G., D'Errico, C., Fallani, L., Fattori, M., Fort, C., Zaccanti, M., Modugno, G., Modugno, M., Inguscio, M.: Anderson Localization of a Non-Interacting Bose-Einstein Condensate. Nature **453**, 895–898 (2008)

11 Abrahams, E., Anderson, P.W., Licciardello, D.C., Ramakrishnan, T.V.: Scaling Theory of Localization - Absence of Quantum Diffusion in 2 Dimensions. Phys. Rev. Lett. **42**, 673-676 (1979)

12 Lukes, T.: Critical Dimensionality in the Anderson-Mott Transition. J. Phys. C **12**, L797 (1979).

13 Kunz, H., Souillard, B.: On the Upper Critical Dimension and the Critical Exponents of the Localization Transition. J. Phys. Lett. **44**, L503-L506 (1983)

14 Straley, J.P.: Conductivity Near the Localization Threshold in the High-Dimensionality Limit. Phys. Rev. B **28**, 5393 (1983)

15 Efetov, K.B. : Anderson Transition on a Bethe Lattice (the Symplectic and Orthogonal Ensembles). Zh. Eksp. Teor. Fiz **93**, 1125–1139 (1987) [Sov. Phys. JETP **61**, 606 (1985)]

16 Castellani, C., DiCastro, C., Peliti, L.: On the Upper Critical Dimension in Anderson Localization. J. Phys. A **19**, 1099-1103 (1986)

17 Zhu, C.P., Xiong, S.-J.: Localization-Delocalization Transition of Electron States in a Disordered Quantum Small-World Network. Phys. Rev. B **62**, 14780 (2000)

18 Giraud, O. , Georgeot, B., Shepelyansky, D.L.: Quantum Computing of Delocalization in Small-World Networks. Phys. Rev. E **72**, 036203 (2005)

19 Gong, L., Tong, P.: von Neumann Entropy and Localization-Delocalization Transition of Electron States in Quantum Small-World Networks. Phys. Rev. E **74**, 056103 (2006)

20 Sade, M., Berkovits, R.: Localization Transition on a Cayley Tree via Spectral Statistics. Phys. Rev. B **68**, 193102 (2003)

21 Sade, M., Kalisky, T., Havlin, S., Berkovits, R.: Localization Transition on Complex Networks via Spectral Statistics. Phys. Rev. E **72**, 066123 (2005)

22 Jahnke, L., Kantelhardt, J.W., Berkovits, R., Havlin, S.: Wave Localization in Complex Networks with High Clustering. Phys. Rev. Lett. **101**, 175702 (2008)

23 Albert, R., Barabási, A.L.: Statistical Mechanics of Complex Networks. Rev. Mod. Phys. **74**, 47-97 (2002)

24 Erdös, P., Rényi, A.: On Random Graphs. Publ. Math. Debrecen **6**, 290-297 (1959)

25 Kalisky, T. , Cohen, R. , ben Avraham, D. , Havlin S.: Tomography and Stability of Complex Networks. In: Ben-Naim, E., Frauenfelder H., Toroczkai Z. (eds) Lecture Notes in Physics: Proceedings of the 23rd LANL-CNLS Conference, "Complex Networks", Santa-Fe, 2003, Springer, Berlin (2004)

26 Cohen, R., Erez, K., ben Avraham, D., Havlin, S.: Resilience of the Internet to Random Breakdowns. Phys. Rev. Lett. **85**, 4626–4628 (2000)

27 Carmi, S., Havlin, S., Kirkpatrick, S., Shavitt, Y., Shir, E.: A Model of Internet Topology using k-Shell Decomposition. PNAS **104** 11150-11154 (2007)

28 Cohen, R., Havlin, S.: Scale-Free Networks are Ultrasmall. Phys. Rev. Lett. **90**, 058701 (2003)

29 Bollobas, B., Riordan, O.: Mathematical Results on Scale-Free Random Graphs. In: Bornholdt, S., Schuster, H.G. (eds.) Handboook of Graphs and Networks. Wiley-VCH, Berlin (2002)

30 Watts, D. J., Strogatz, S. H.: Collective Dynamics of 'Small-World' Networks. Nature **393**, 440-442 (1998)

31 Newman, M. E. J.: Assortative Mixing in Networks. Phys. Rev. Lett. **89**, 208701 (2002)

32 Serrano, M. A., Boguñá, M.: Percolation and Epidemic Thresholds in Clustered Networks. Phys. Rev. Lett. **97**, 088701 (2006)

33 Serrano, M. A., Boguñá, M.: Clustering in Complex Networks. I. General Formalism. Phys. Rev. E **74**, 056114 (2006)

34 Serrano, M. A., Boguñá, M.: Clustering in Complex Networks. II. Percolation Properties. Phys. Rev. E **74**, 056115 (2006)

35 Vázquez, A., Pastor-Satorras, R., Vespignani, A.: Large-Scale Topological and Dynamical Properties of the Internet. Phys. Rev. E **65**, 066130 (2002)

36 Serrano, M. A., Boguñá, M.: Tuning Clustering in Random Networks with Arbitrary Degree Distributions. Phys. Rev. E **72**, 036133 (2005)

37 Dorogovtsev, S. N., Mendes, J. F. F.: Evolution of Networks – From Biological Nets to the Internet and WWW. Oxford University Press, Oxford (2003)

38 Pastor-Satorras, R., Vespignani A.: Evolution and Structure of the Internet : A Statistical Physics Approach. Cambridge University Press, Cambridge (2004)

39 Molloy, M., Reed, B.: The Size of the Giant Component of a Random Graph with a Given Degree Sequence. Combinatorics, Probability & Computing **7**, 295–305 (1998).

40 Cohen, R., Erez, K., ben Avraham, D., Havlin, S.: Breakdown of the Internet under Intentional Attack. Phys. Rev. Lett. **86**, 3682–3685 (2001)

41 Cohen, R., ben Avraham, D., Havlin, S.: Percolation Critical Exponents in Scale-Free Networks. Phys. Rev. E, **66**, 036113 (2002)

42 Barabási, A. L., Albert, R.: Emergence of Scaling in Random Networks. Science **286**, 509 (1999)

43 Volz E.: Random Networks with Tunable Degree Distribution and Clustering. Phys. Rev. E, **70**, 056115 (2004)

44 Kantelhardt, J. W., Bunde, A.: Sublocalization, Superlocalization, and Violation of Standard Single Parameter Scaling in the Anderson Model, Phys. Rev. B **66**, 035118 (2002)

45 MacKinnon, A., Kramer, B.: One-Parameter Scaling of Localization Length and Conductance in Disordered Systems. Phys. Rev. Lett. **47**, 1546–1549 (1981).

46 Slevin, K., Ohtsuki, T., Kawarabayashi, T.: Topology Dependent Quantities at the Anderson Transition, Phys. Rev. Lett. **84**, 3915–3918 (2000)

47 Shapiro, B.: Renormalization-Group Transformation for the Anderson Transition. Phys. Rev. Lett., **48**, 823–825 (1982)

48 Anderson, P. W., Thouless, D. J., Abrahams, E., Fisher, D.S.: New Method for a Scaling Theory of Localization. Phys. Rev. B, **22**, 3519-3526 (1980)

49 Edrei, I., Kaveh, M., Shapiro, B.: Probability-Distribution Functions for Transmission of Waves Through Random-Media – a new Numerical-Method. Phys. Rev. Lett., **62**, 2120–2123 (1989)

50 Khmel'nitskii, D. E., Larkin, A. I.: Mobility Edge Shift in External Magnetic Field. Solid State Commun. **39**, 1069 (1981)

51 Jahnke, L., Kantelhardt, J.W., Berkovits, R., The Effect of a Small Magnetic Flux on the Metal-Insulator Transition. Preprint (2009)

52 Hofstadter, D. R.: Energy Levels and Wave Functions of Bloch Electrons in Rational and Irrational Magnetic Fields. Phys. Rev. B **14**, 2239 (1976)

53 Wigner, E. P.: On a Class of Analytic Functions from the Quantum Theory of Collisions. Ann. Math. **53**, 36 (1951)

54 Dyson, F. J.: Statistical Theory of the Energy Levels of Complex Systems. J. Math. Phys. **3**, 140 (1961)

55 Efetov, K. B.: Supersymmetry and Theory of Disordered Metals. Adv. Phys. **32**, 53 (1983)

56 Altshuler, B. L., Shklovskii, B. I.: Repulsion of Energy-levels and the Conductance of Small Metallic Samples. Sov. Phys. JETP **64**, 127 (1986)

57 Altshuler, B. L., Zharekeshev, I. Kh., Kotochigova, S. A., Shklovskii, B. I.: Energy-level Repulsion and the Metal-Insulator-Transition. Sov. Phys. JETP **67**, 625 (1988)

58 Shklovskii, B. I., Shapiro, B., Sears, B. R., Lambrianides P., Shore H. B.: Statistics of Spectra of Disordered-Systems near the Metal-Insulator-Transition. Phys. Rev. B, **47**, 11487-11490 (1993)

59 Hofstetter E., Schreiber M.: Relation between energy-level statistics and phase transition and its application to the Anderson model. Phys. Rev. E, **49**, 14726 (1994)

60 Metha, M. L.: Random matrices. Academic Press, Boston (1991)

61 Guhr, T., Müller-Groeling, A., Weidenmüller, H. A.: Random-Matrix Theories in Quantum Physics: Common Concepts. Phys. Rep. **299**, 189 (1998)

62 Mirlin, A. D., Statistics of Energy Levels and Eigenfunctions in Disordered Systems. Phys. Rep. **326**, 260 (2000)

63 Schreiber, M., Grussbach, H.: Dimensionality Dependence of the Metal-Insulator Transition in the Anderson Model of Localization. Phys. Rev. Lett., **76**, 1687-1690 (1996)

64 Meir, Y., Aharony, A., Harris, A. B.: Delocalization Transition in Two-Dimensional Quantum Percolation. Europhys. Lett. **10**, 275 (1989)

65 Taylor, J. P. G., MacKinnon, A.: A Study of the Two-Dimensional Bond Quantum Percolation Model. J. Phys. Condens. Mat. **1**, 9963 (1989)

66 Koslowski, T., v. Niessen, W.: Mobility Edges for the Quantum Percolation Problem in Two and Three Dimensions. Phys. Rev. B **42**, 10342 (1990)

67 Soukoulis, C. M., Grest, G. S.: Localization in Two-Dimensional Quantum Percolation. Phys. Rev. B **44**, 4685 (1991)

68 Soukoulis, C. M., Li, Q., Grest, G. S.: Quantum Percolation in Three-Dimensional Systems. Phys. Rev. B **45**, 7724 (1992)

69 Dasgupta, I., Saha, T., Mookerjee, A.: Analysis of Stochastic Resonances in a Two-Dimensional Quantum Percolation Model. Phys. Rev. B **47**, 3097 (1993).

70 Berkovits, R., Avishai, Y.: Spectral Statistics Near the Quantum Percolation Threshold. Phys. Rev. B **53**, R16125-R16128 (1996)

71 Kusy, A., Stadler, A. W., Haldas, G., Sikora, R.: Quantum Percolation in Electronic Transport of Metal-Insulator Systems: Numerical Studies of Conductance. Physica A **241**, 403 (1997).

72 Kaneko, A., Ohtsuki, T.: Three-Dimensional Quantum Percolation Studied by Level Statistics. J. Phys. Soc. Jpn. **68**, 1488 (1999)

73 Lorenz, C.D., Ziff, R.M.: Precise Determination of the Bond Percolation Thresholds and Finite-Size Scaling Corrections for the sc, fcc, and bcc Lattices. Phys. Rev. E, **57**, 230-236 (1998)

74 Alexander, S., Orbach, R.: Density of States on Fractals: Fractons. J. Phys. (Paris) Lett. **43**, L-625 (1982)

75 Slevin, K., Ohtsuki, T.: The Anderson Transition: Time Reversal Symmetry and Universality. Phys. Rev. Lett. **78**, 4083–4086 (1997)

76 Kawarabayashi, T., Kramer, B., Ohtsuki, T.: Anderson Transitions in Three-Dimensional Disordered Systems with Randomly Varying Magnetic Flux. Phys. Rev. B **57**, 11842–11845 (1998)

Index

Anderson model, 10, 20
assortativity, 6

boundary conditions, 20, 25

clustering, 5, 8, 23
complex system, 1
critical exponent, 11, 22, 23

degree distribution, 3, 8
dynamical matrix, 11

finite-size scaling, 19

Hamiltonian, 10

level statistics, 16, 21
localization, 1, 21
localization-delocalization transition, 1, 10, 17, 21, 27

magnetic field, 14, 25

optical modes, 13, 23
optical network, 13

percolation, 7, 11, 21
phase transition, 1, 21
photonic lattice, 14
Poisson distribution, 3, 17
power law, 3, 11, 15

quantum percolation, 11

random matrix theory, 16

scale-free network, 3, 23
scaling theory, 13, 15, 19
small-world network, 3, 22

tight-binding equation, 10

universality class, 7, 10, 27

vibrational modes, 11

Wigner distribution, 16